ORIGINAL ARTICLE

Effect of exfoliated MoS$_2$ on the Microstructure, Hardness, and Tribological Properties of Copper Matrix Nanocomposite Fabricated via the Hot Pressing Method

Hossam M. Yehia[1] · Ahmed I. Ali[2,3] ·
Ehab Abd-Elhameed[4]

Abstract In this study, copper matrix composites were prepared using the cold and hot pressing technique and then investigated to select the suitable one for the self-lubricating applications. A hybrid of alumina and molybdenum disulfide with a 1:1 ratio by the mechanical milling for 40 h was proceeded to peel the molybdenum disulfide and cover the alumina particles with their layers. Three different samples like Cu, Cu/10 Al$_2$O$_3$, and Cu/hybrid 20(Al$_2$O$_3$–MoS$_2$) were mixed for 15 h. The ball-to-powder ratio in the two mentioned steps was 10:1. The X-ray analysis, HRTEM, Raman spectra, and scanning electron miscopy were used to study the crystal structure, chemical composition, and morphology of the new hybrid and prepared samples. The density was evaluated by the Archimedes method. Mechanical properties, including hardness, wear rate, and coefficient of friction, were investigated. The mixing for 15 h improves the exfoliation of MoS$_2$ flakes inside the copper matrix. A clear hardness improvement was achieved by adding alumina and the mixture of (Al$_2$O$_3$–MoS$_2$). The copper sample reinforced with the hybrid of alumina/MoS$_2$ gave the lowest mechanical wear rate and the lowest average friction coefficient of 0.17.

1 Introduction

The loss of energy due to friction associated with the movement of mechanical assembly parts (MMAP) is a fundamental problem in industrial applications. The problem is related to the presence of friction and the occurrence of mechanical wear, which reduces the service time for the used parts and the need to replace them, thus the consumption and loss of time for business owners. The primary energy loss due to friction has been estimated to be 30%, and billions of corresponding financial losses have been evaluated [1]. For this reason, we thought of producing self-lubricating materials resisting repeated mechanical loss of parts that results from insufficient lubrication, especially in harsh friction conditions where lubricating fluids are unsuitable. The most common metallic materials used to produce self-lubricating materials in this application are copper, silver, gold, lead, tin, and platinum. Since copper has high flexibility that makes it easy to form and has high thermal conductivity, it is widely used in such applications. Copper matrix composites reinforced with solid lubricants such as graphite, MoS$_2$, and WS$_2$ have been widely used as self-lubricating in many applications such as bearings and bushings for their low friction coefficient and high wear-resistant properties [2–6]. Nevertheless, copper suffers from poor mechanical wear resistance. Molybdenum disulfide is a solid lubricant material. It is similar in its structure to graphite, as it consists of flakes whose atoms Mo and S are linked with a covalent bond, which indicates the strength of the contact between them, as is the case in graphene layers. The schematic diagram of

✉ Hossam M. Yehia
  hossamelkeber@techedu.helwan.edu.eg

1 Production Technology Department, Faculty of Technology and Education, Helwan University, Saray–El Qoupa, El Sawah Street, Cairo 1128, Egypt

2 Basic Science Department, Faculty of Technology and Education, Helwan University, Saray–El Qoupa, El Sawah Street, Cairo 11281, Egypt

3 Nanotechnology Research Center, The British University in Egypt (BUE), El Sherouk City, Suez Desert Road, Cairo 11837, Egypt

4 El-Sahafa Institute, Ministry of Higher Education, Cairo, Egypt

the MoS_2 structure with details of the lattice parameters is shown in Fig. 1 [7].

The MoS_2 can provide lubrication for moving parts such as graphite, especially in a vacuum and dry gas environment. It has a lamellar structure such as graphite formed by many stacked layers. Each MoS_2 layer is composed of a plane of molybdenum embedded between two planes of sulfur atoms by the covalent bonds. Therefore, the strength of every single layer is high as graphene [8, 9]. Some studies on copper matrix composites strengthened with MoS_2 were performed to improve their tribological performance. Reinforcing the copper matrix with 10 wt% MoS_2 increased the hardness to 89HV with a 32.83% increment. The wear rate dramatically decreased from 0.04 to 0.02 g, and the coefficient of friction reduced to 0.32 μm [10]. Jin-Kun Xiao et al. [11] investigated the tribological behavior of Cu–MoS_2 composites. The results confirmed that MoS_2 addition was an effective lubricant for copper matrix composites against steel. The friction coefficient decreased from 0.67 to 0.18 when added 20 Vol% of the MoS_2. The wear rate of the composites tended to increase at low percentages and then reduced as the MoS_2 content increased. Researchers have tried to improve the properties of the copper-based materials by reinforcing them with ceramic materials such as Al_2O_3, ZrO_2, TiC, WC, or SiC [12–18]. The presence of ceramic particles in the matrix (bushings) destroys the shaft surface (the protected parts) by scratching it. The authors suggested coating the ceramic particles with MoS_2 layers to solve the problem. Coating the alumina particles with the molybdenum disulfide flakes will cover the sharp edges, reduce their surface roughness, and, consequently, the coefficient of friction and mechanical wear. From the authors' point of view, this will improve the strength and resistance of the materials to erosion and thus increase their service life. In addition, maintaining the essential parts required to be protected from mechanical wear (shaft or machine frame).

Hybrid materials have advantages over single materials when manufactured, especially when they contain two-dimensional or one-dimensional materials. Researchers confirmed that the presence of two- or one-dimensional materials such as graphene and carbon nanotubes (CNTs) in composites could improve strength and stability due to their superior mechanical, thermal, electrical, and chemical properties [19–22].

This study aims to exfoliate the molybdenum disulfide to flakes and use it with alumina to strengthen the copper matrix to reduce the rate of mechanical wear and coefficient of friction, consequently increasing the life of copper composites that are used as self-lubricating bushings. The chemical composition, morphology, densification, hardness, mechanical wear, and coefficient of friction of fabricated copper matrix nanocomposites have been studied.

2 Materials and Methods

In this study, the as-received molybdenum disulfide powder (MoS_2) of the mean particles size 1–0.5 μm was supplied by the DOP ORGANİK KİMYA SAN. VE TİC. LTD ŞTİ, the nano-Al_2O_3 powder with mean particles size 200–500 nm (Hart Minerals) and the copper powder of 1–3 μm (OXFORD Laboratory Reagent; India) were used to fabricate copper matrix nanocomposite for lubricant applications. A die with an inner diameter of 16 mm and 60 mm high fabricated from W320 alloy steel has been used for the

Fig. 1 **a** MoS_2 atomic structure (black and yellow spheres representing the Mo and S atoms, respectively), **b** top view (honeycomb lattice), and **c** lateral view of MoS_2
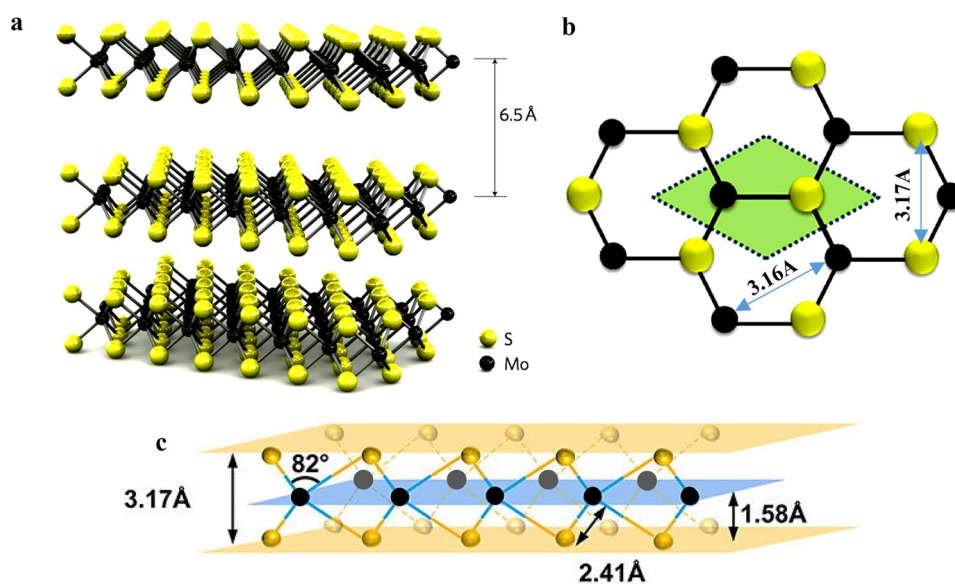
hot forming process. The outside diameter of the used die was 50 mm.

The Al_2O_3 and MoS_2 with a 1:1 ratio were mixed for 40 h to exfoliate MoS_2 layers and coat the Al_2O_3 particles. The process was performed at 150 rpm with a 1:10 powder-to-ball ratio in an uncontrolled atmosphere. A ceramic alumina ball with a 12 mm diameter was used. The machine was stopped each 30 min for 10 min to maintain the powder at room temperature. *Three copper nanocomposites:* Cu, Cu/10 Al_2O_3, and Cu/hybrid (10 Al_2O_3–10 MoS_2), were prepared by mechanical alloy milling for 15 h. The prepared nanocomposites were cold-pressed at 1000 MPa and then heated to 750 °C for 35 min; after that, they were hot-pressed at 1000 MPa. A 70-ton hydraulic press was used to perform the compaction process. Production steps are summarized in Fig. 2. The hardness of the three samples was studied by the Vickers tester (NEMESIS 9100 at 3 kg for 10 s). The

wear rate by the pin on a ring test rig at 2.6 m/sec for 10 min loading time and different loads (40 and 50 N) was studied. The coefficient of friction was evaluated at the same time.

3 Characterizations

The morphology of the fabricated samples was investigated using scanning electron microscopy (FE-SEM (EBS mode) model Quanta FEG250. The structure of the samples was investigated using X-ray diffraction. The X-ray diffraction patterns were measured via the diffractometer (Bruker: D8) through (CuKα; $\lambda \sim 1.540$ Å), employed at ~40 mA/42 kV. The X-rays were completed through an angular range from $2\theta = 10°$ to 80°. The Confocal Raman spectroscopy Model Witec (laser excitation 532 nm) was used to check the transformation of the GNs. The density of the samples was measured using the Archimedes' route according to MPIF standards 42, 1998.
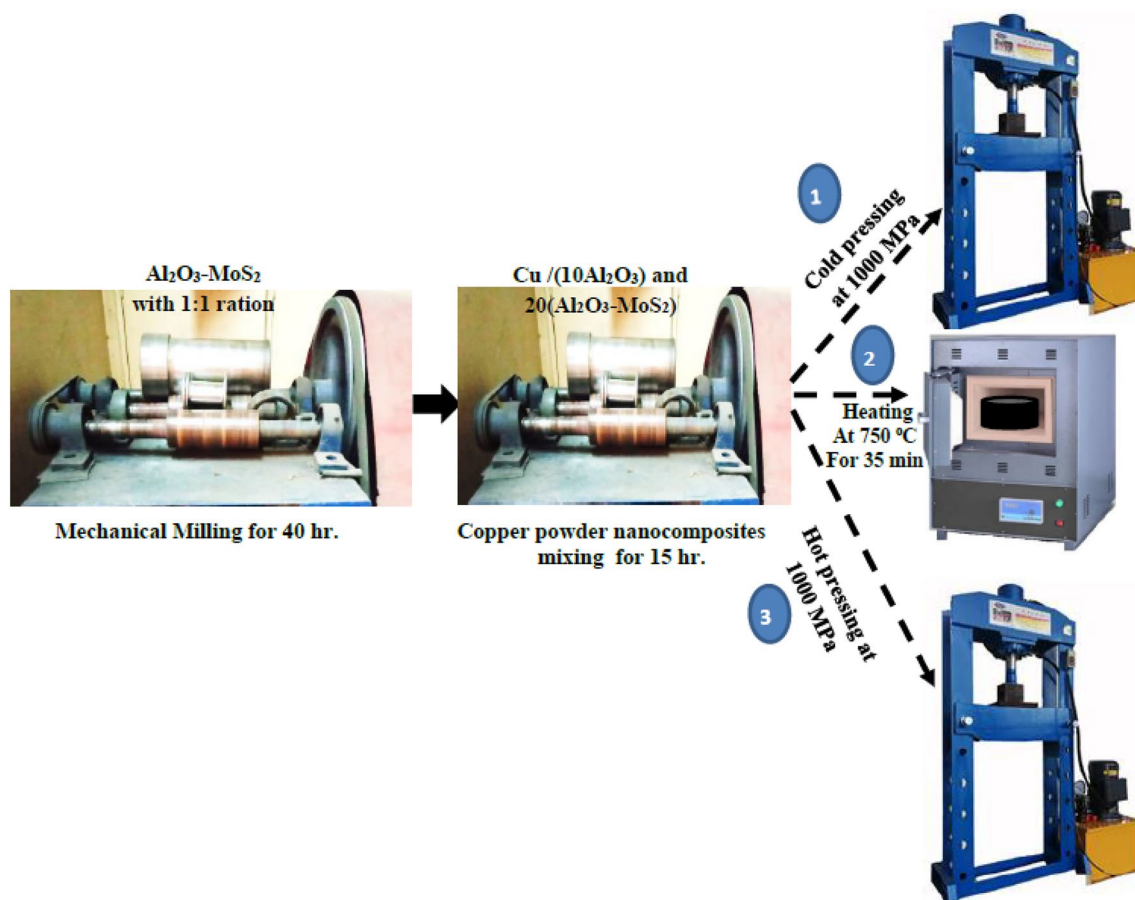

Fig. 2 Schematic diagram of the process adopted for development of the composites

4 Result and Discussion

4.1 Raman and HRTEM of the Hybrid (Al$_2$O$_3$–MoS$_2$) Powder

In this study, the number of exfoliated MoS$_2$ due to the mechanical alloy milling with alumina with a 1:1 ratio was investigated by the Raman analysis, as shown in Fig. 3a. The number of layers has been determined from a distance between two fingerprint peaks (observed at ∼383 cm^{-1} and ∼408 cm^{-1} in bulk MoS$_2$ [23]). With the increasing number of single layers, the mode at ∼383 cm^{-1} shifted to lower frequencies, and the mode at ∼408 cm^{-1} changed to higher frequencies (Fig. 3b). The analysis detected the peaks of the MoS$_2$ at 378 and 403 cm^{-1} which means an incomplete conversion of MoS$_2$ to nanolayers at the mentioned weight percentages. No peaks for the molybdenum trioxides MoO$_3$ were detected at 820 cm^{-1} according to the reference in Fig. 1c [24], indicating no transition of MoS$_2$ to MoO$_3$. In addition to molybdenum peaks, alumina peaks have been also discovered.

The HRTEM micrograph of the hybrid (MoS$_2$–Al$_2$O$_3$) powder is shown in Fig. 4. A separation of the MoS$_2$ occurred. Single layers with an enormous surface area were observed. Also, free MoS$_2$ layers were detected. Due to the mechanical milling for a long time, 40 h, a crystallite

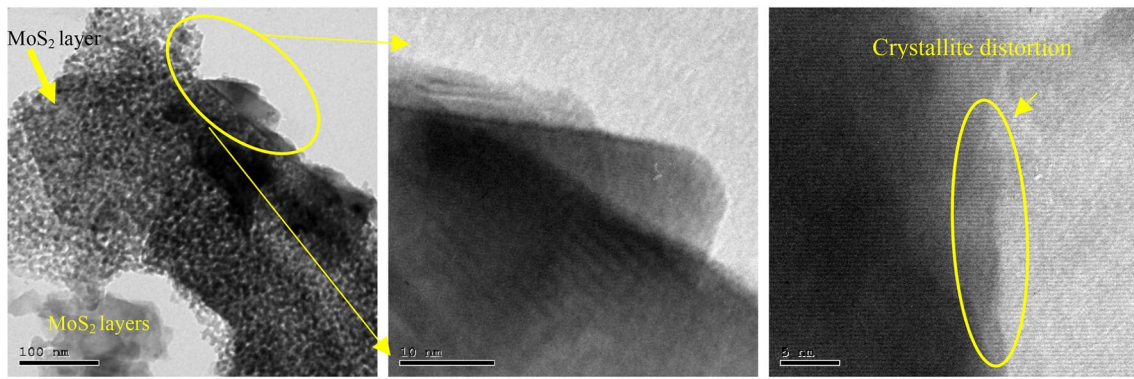**Fig. 3** Raman analysis of the hybrid (MoS$_2$–Al$_2$O$_3$)
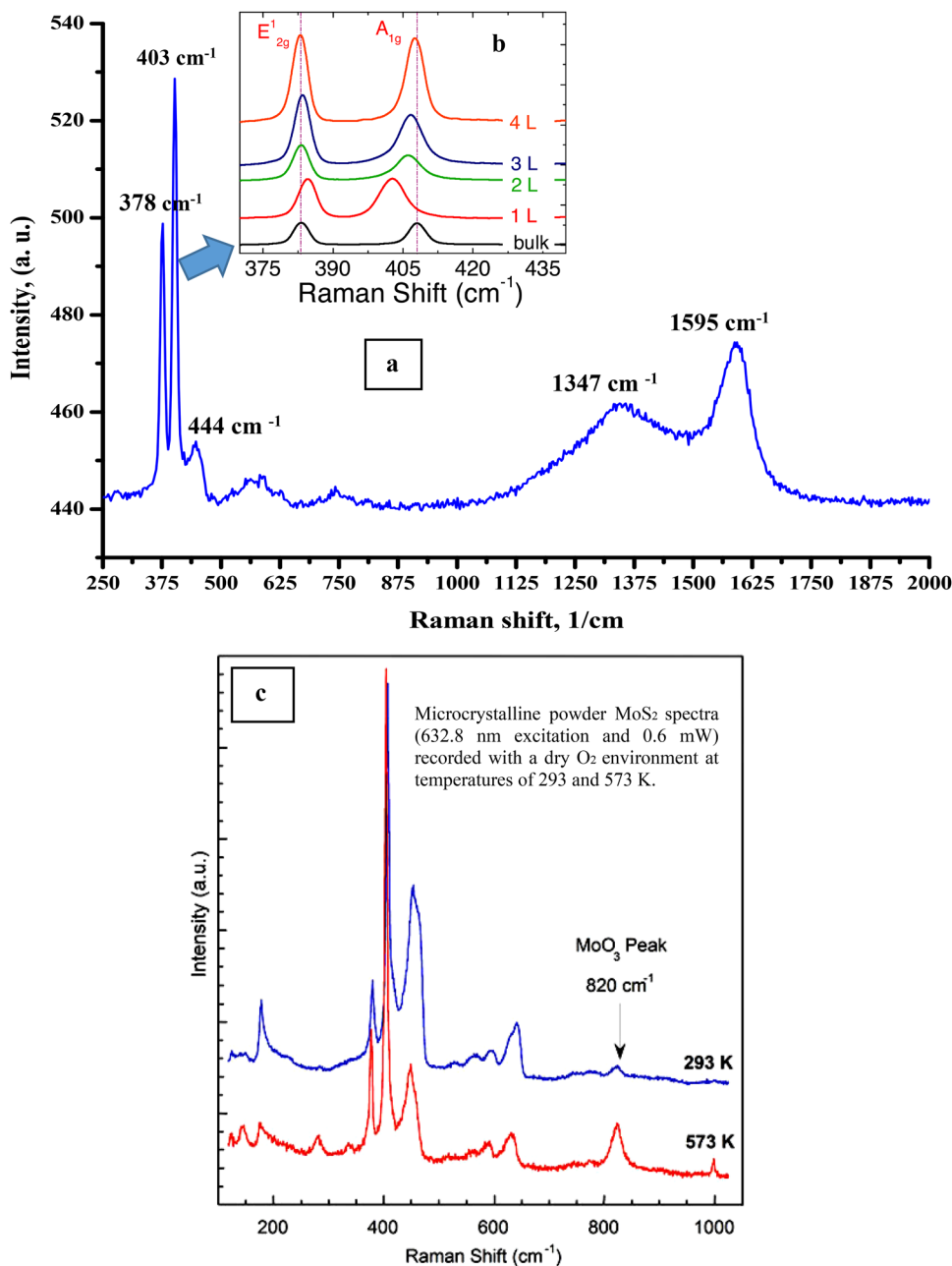
Fig. 4 HRTEM of the hybrid (MoS$_2$–Al$_2$O$_3$)

distortion was detected. A benefit can be gained from the phenomenon, where the crystallite distortion may reduce dislocation movement and grain slipping, consequently increasing reinforced material strength.

4.2 X-ray Diffraction

The crystal structure of the hot compacted copper nanocomposites was examined by the X-ray analysis, as shown in Fig. 5. In the frits sample, copper and copper oxide of the cubic crystal structures have been detected. The copper oxide peaks did not appear. This means the structure is a single phase. By adding 10 wt% Al$_2$O$_3$, the crystal structures transited to the tetragonal phase (second sample). One can note here that the peak of the copper oxide CuO is detectable. The copper oxide peak was reduced in the third sample due to coating Al$_2$O$_3$ particles by

the MoS$_2$ layers. The molybdenum trioxides MoO$_2$ was detected, which may be formed due to exposing the MoS$_2$ layers to heat during the hot pressing process. The Molybdenum disulfide (MoS$_2$) and molybdenum trioxide were studied using Raman spectroscopy [24]. Transformation of MoS$_2$ to MoO$_3$ was detected due to the laser intensity effects. The transformation to molybdenum trioxide was interpreted as a function of temperature and atmosphere, revealing an apparent transformation at 375 K in the presence of oxygen. A reduction in the copper peak intensities and increased peak broadening were detected. Increasing the peak broadening indicates decreasing the copper particles' size due to the mechanical milling for 15 h. No intermetallic compounds were detected. This may be due to performing the fabrication process at a low temperature of 750 °C and low heating time.

Fig. 5 X-Ray patterns of copper nanocomposites fabricated by hot compaction
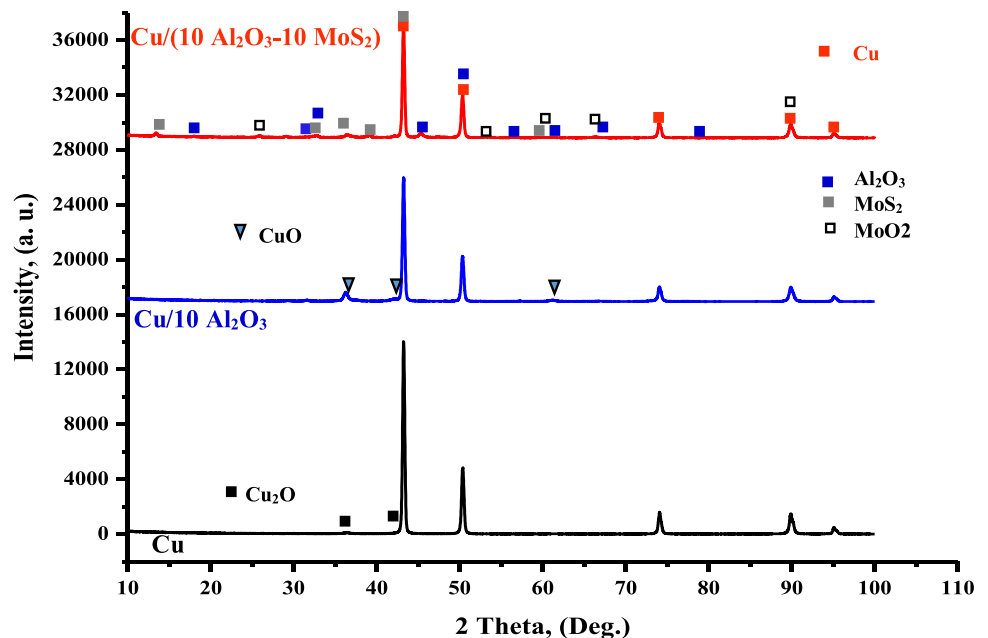
4.3 Densification

Figure 6 represents the relative density of the copper matrix nanocomposites. Under the mentioned fabrication condition, the pure copper sample achieved 92.5% relative density. Applying high pressure on cold and hot increased the adhesion between copper particles, which led to the absence of voids, thus achieving a high density of 92.5% at a low temperature of 750 °C. Because alumina has a low density of 3.95 g/cm^3 compared to copper (8.9 g/cm^3), its addition led to a decrease in the density of copper. The third sample had the same behavior as sample 2. The density of the hybrid $10Al_2O_3 + 10MoS_2$ (4.505 g/cm^3) is less than that of copper (8.9 g/cm^3), which led to a decrease in the density of the new compound in general. This reduction can be explained by the fact that the particles of the lighter materials replace the particles of the higher density materials, leading to a wholly decreased density. Another factor that could explain the reduction in density of the copper matrix is the formation of pores between the base metal and the supporting material. Also, the formation of oxides Cu_2O, CuO, and MoO_2 detected from the x-ray analysis may affect the matrix density, as it has a density less than that of the pure metal.

4.4 Microstructure

Figure 7 shows the morphology of the copper, MoS_2, and alumina initial raw materials used and the fabricated Cu, Cu/10 Al_2O_3, and Cu/(10 Al_2O_3–10 MoS_2) nanocomposites, respectively. The microstructure of the reinforcement powders shows that the copper has a dendritic shape, MoS_2 has flake shape particles, and alumina has a semispherical shape. The fabricated pure copper sample shows complete diffusion between some particles of copper. Black areas on the grain boundaries represent the copper oxide formed during the fabrication process, possibly due to the hot forming process in an uncontrolled atmosphere. Due to addition of 10 wt% alumina to the second sample and milling for 15 h, a refining of copper particles was observed. The particles' refining maybe also due to the high application pressure before and after heating. This process can be classified under severe plastic deformation according to the microstructure. The black areas represent the copper oxide increase due to the reaction between copper and alumina and the refining of particles that increase the contact area. The third sample showed high diffusivity of molybdenum flakes with the copper matrix. The microstructure proved the separation of molybdenum in the form of flakes. The MoS_2 layers in the last image d appeared transparent and took the horizontal position.

4.5 Hardness

The effect of 10 wt% nano-Al_2O_3 and hybrid $20(Al_2O_3$–$MoS_2)$ on the hardness of the copper matrix is shown in Fig. 8. The copper matrix recorded 96.1 HV, nearly equal to the expected value of copper (100 HV). Reinforcing the copper with 10 wt% nano-Al_2O_3 increased the hardness to 150.47 HV, equivalent to a 56.5% improvement in the hardness of pure copper. Alumina is characterized by high hardness and strength compared to carbides and metals. The effect of alumina content up to 15 wt% on the hardness of copper matrix was studied. Hardness was evaluated by the Brinell hardness method. The hardness of copper was increased gradually from 45HB for pure copper to 60, 70, and 75 HB by adding 5, 10, and 15 wt%Al_2O_3. Authors attributed this improvement to the higher constraint to the localized matrix deformation during indentation due to the presence of Al_2O_3. Due to producing some agglomerations at 15 wt% Al_2O_3, the increment was more minor than at 5

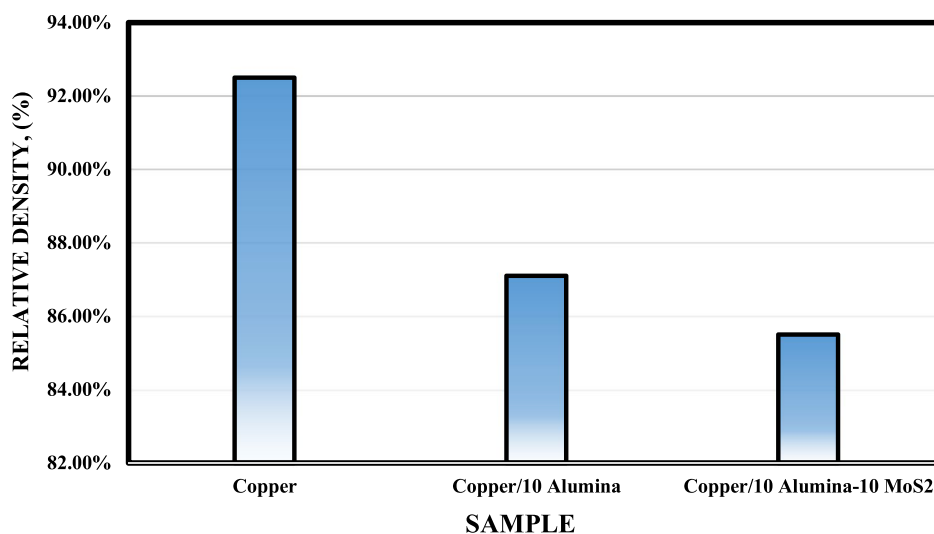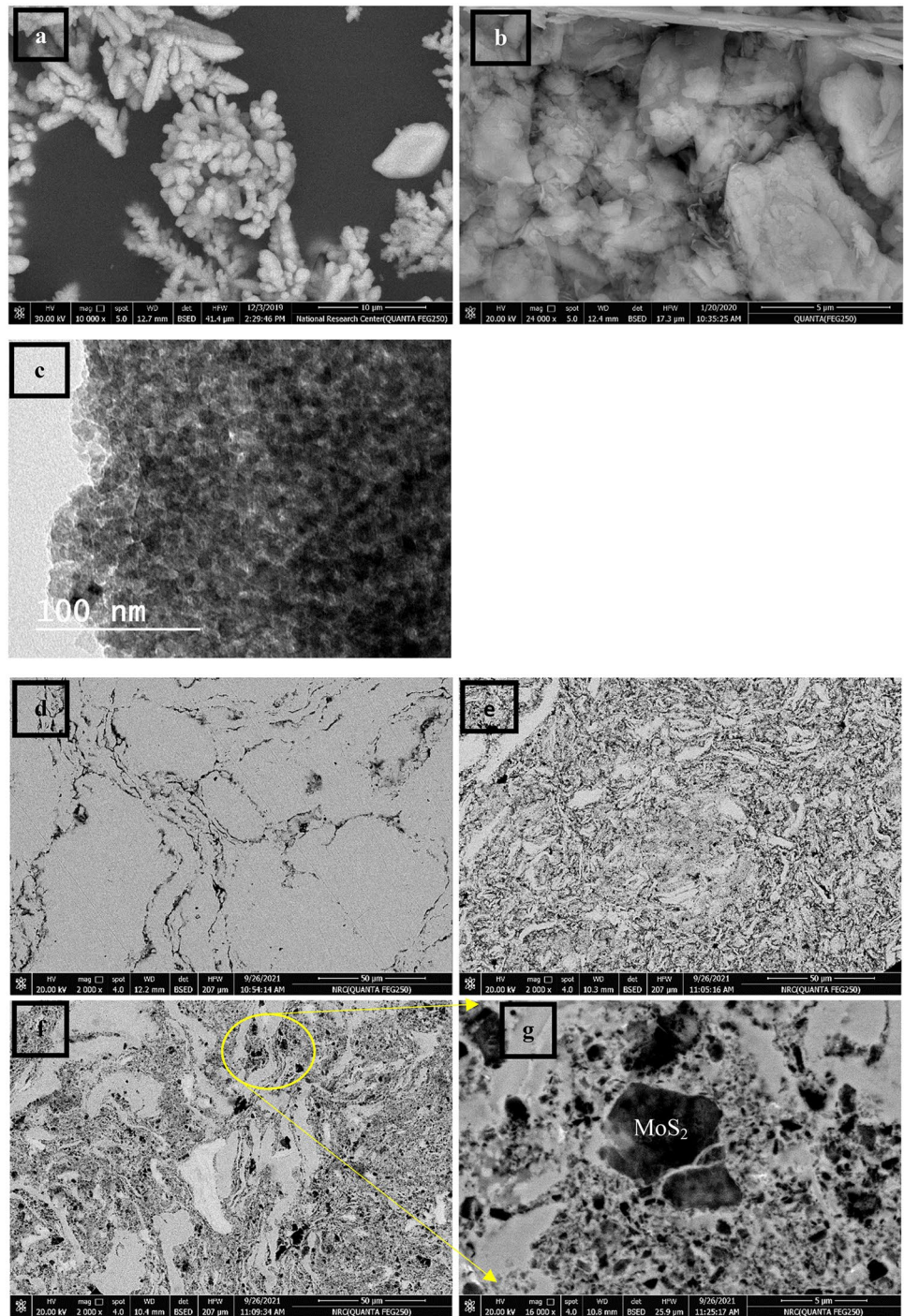**Fig. 6** Relative density of fabricated capper nanocomposites

Fig. 7 Microstructure of the initial raw materials used and hot-pressed copper matrix nano-composites **a** copper powder, **b** MoS$_2$ powder, **c** alumina powder, **d** solid pure copper, **e** Cu/10 Al$_2$O$_3$, and (**f** and **g**) Cu/20(Al$_2$O$_3$–MoS$_2$)

and 10 wt%Al$_2$O$_3$ [25]. Due to exfoliating the MoS$_2$ into layers and spreading it with alumina in the copper matrix, the third sample recorded 175.45 HV, which is equivalent to an increase in the hardness by 16.6% compared to the Cu/10 Al$_2$O$_3$ sample, and by 82.57% compared to the pure copper sample. The correlation between density and hardness of the selective laser melting (SLM) of AISI 316L was investigated. In general, the better the density of the material, the more promising its mechanical properties. The increased microhardness of AISI 316L with a higher density is due to their associated lower porosity. A higher relative density leads to a higher portion of the material being available to offset the indentation of the test sample during hardness measurements. Also, relative density increases the material's resistance against deformation and thus increases microhardness [26]. Although the relative density deteriorated with the addition of 10% Al$_2$O$_3$ and 20% (Al$_2$O$_3$ + MoS$_2$), copper hardness got significantly improved. This can be
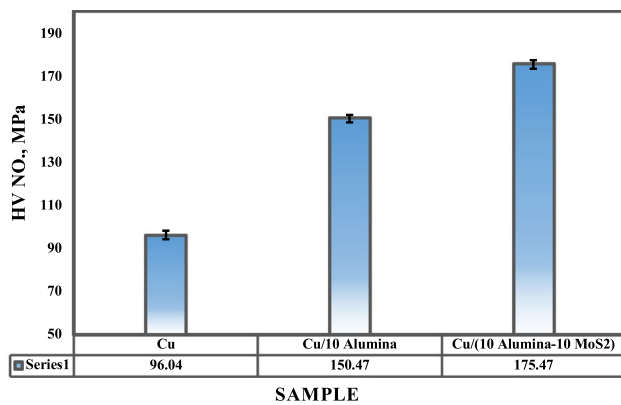
Fig. 8 Macro-hardness of hot-pressed samples

Fig. 9 Wear rate of hot-pressed copper nanocomposites at 40 and 50 N

interpreted by some factors related to the matrix's reinforcement, distribution, and adhesion characteristics. As mentioned, alumina has high hardness. Adding the MoS_2 to the Al_2O_3 with a 1:1 ratio and mixing them for 40 h and 15 h with copper participated in peeling it into flakes, as shown from the HRTEM in Fig. 4 and the microstructure in the last image, Fig. 7f. Peeling the MoS_2 into layers changes its properties where it becomes more strong. The microstructure shown in Fig. 7 demonstrates that the MoS_2 layers took horizontal and arbitrary orientations. The horizontal position made the copper matrix resist the penetration of the indenter during the hardness test. An excellent distribution of the MoS_2 layers was observed from the microstructure. The hardness property of copper matrix composites reinforced with hybrid (1.5CNTs–0.5Al_2O_3) was studied [27]. The result of Vickers hardness shows that reinforcing copper with 0.5 wt% Al_2O_3 increased its hardness to 115 HV while reinforcing it with hybrid (1.5CNTs–0.5Al_2O_3) increased it to 131 HV. It has been found that the integration of CNTs and/or Al_2O_3 dramatically increases the tensile strength while it decreases the elongation of the copper matrix. The addition of 1.5CNTs–0.5Al_2O_3 established the highest ultimate tensile strength of 345 MPa. The effect of reinforcing Al–5Ni–0.5 Mg with different percentages of 2.5, 5, and 7.5 wt% of (Al_2O_3–GN) was investigated [28]. The Al–5Ni–0.5 Mg/7.5 wt% of (Al_2O_3–GN) sample recorded 98 HV compared with 56 HV for the matrix alloy Al–5Ni–0.5 Mg. 42.8% improvement in the hardness has been achieved. Applying the pressure before and after heating had a significant effect, where it reduced the particle size under high shearing processes and increased the adhesion between interparticles, as shown in Fig. 6f. The reinforcement particle size influences the strength of materials. The HRTEM in Fig. 5 shows that alumina has a nanosize. Reducing the particle size increases the area of contact and, consequently, the strength and hardness of reinforced material.
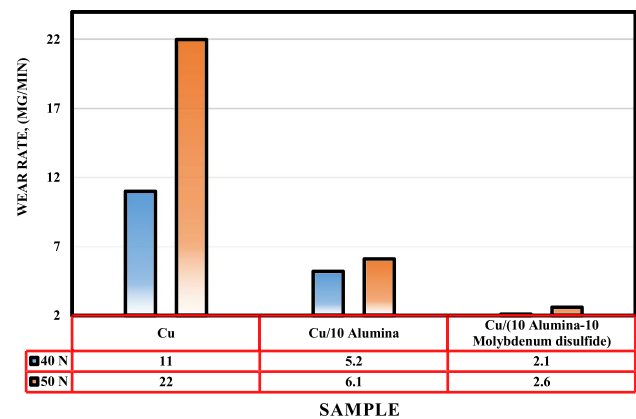
Also, exfoliating the MoS_2 into layers decreases its thickness and increases its surface area.

4.6 Wear rate

The wear rate of the hot-pressed copper nanocomposites at 40 and 50 N for 10 min is shown in Fig. 9. The results showed that the wear rate was decreased by reinforcing the copper matrix with 10 wt% nano–Al_2O_3 and hybrid (10 Al_2O_3–10 MoS_2), respectively. Adding 10 wt% Al_2O_3 to the copper matrix reduced the wear rate by 52.72% and 80.9% when the hybrid was added. The addition of alumina increases the copper hardness and abrasion, which decreases the wear rate. The presence of alumina particles with the copper reduces the influence of the adhesive wear when sliding against a steel disk face. The effect of 5, 10, and 15 wt % Al_2O_3 addition on the wear rate of the copper matrix was studied [25]. Due to the strong particulate matrix bonding and high hardness of the Al_2O_3 particulates, the abrasive wear results demonstrated that the wear rate of the copper decreased with increasing the reinforcement weight fraction. Coating alumina particles with the MoS_2 layers decreased surface roughness, and the movement became smooth; consequently, the wear rate decreased. Also, free MoS_2 layers with the copper matrix and its accumulation on the disk's surface during contact with the pin facilitate the pin sliding and consequently reduce the wear rate. Increasing the strength of the fabricated copper material is due to reducing the particle size during forming processes, and the separation of MoS_2 into layers significantly reduced the wear rate. The wear behavior of copper matrix composites has been evaluated to determine the optimal additive content of MoS_2 with copper [29]. 40 vol% of MoS_2 was added in step 10. Due to the formation of a continuous lubricating film on the worn surface of composites containing MoS_2 above 20 vol%, a
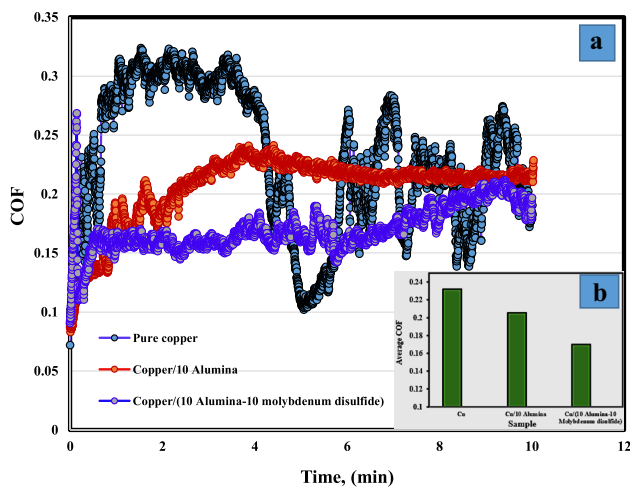
Fig. 10 Friction coefficient of hot-pressed copper nanocomposites at 50 N

decrease in the wear rate was observed. On the other hand, the wear rate was increased by increasing the load due to increasing the contact area between the pin and disk.

4.7 COF

Figure 10 shows the friction coefficient of Cu, Cu/10Al$_2$O$_3$, and Cu/(10Al$_2$O$_3$ –10MoS$_2$) nanocomposites under 50 N applied load. The COF curves of Cu composites are shown in Fig. 10a. It is observed that pure copper exhibited a significantly high COF with an extensive range of inconstancy with increasing time. Integrating Al$_2$O$_3$ and hybrid (Al$_2$O$_3$–MoS$_2$) with the copper matrix effectively decreased the COF. The COF curves dropped and became more stable by adding of 10 wt% nano-Al$_2$O$_3$ and combination (10Al$_2$O$_3$–10MoS$_2$), respectively. The high and oscillate COF of pure copper may be due to the severe adhesion and strain hardening of pure copper at the surface of the contacting pairs. The reduction in COF may be related to the accumulation of the MoS$_2$ layer on the sliding surface, which acts as a solid lubricant and consequently prevents direct contact between the frictional surfaces. The variation of average COF versus the Cu, Cu/10Al$_2$O$_3$, and Cu/20(Al$_2$O$_3$–MoS$_2$) is plotted in Fig. 7b. The average COF was decreased by adding alumina and molybdenum disulfide to the copper matrix. The COF started at 0.2318 for the pure copper and then dramatically reduced by adding alumina to 0.2059. Adding hybrid 20(Al$_2$O$_3$–MoS$_2$) reduced the COF to 0.17 by a 26.66% reduction compared with pure copper.

The effect of 0.5 wt% Al$_2$O$_3$ and hybrid (1.5CNTs–0.5Al$_2$O$_3$) addition on the COF of the copper matrix were studied [26]. The Al$_2$O$_3$ addition in the copper matrix increased the COF while the hybrid 0.5CNTs–0.5Al$_2$O$_3$ decreased and remained stable (~0.155).

Authors attributed the increase in the COF by adding the Al$_2$O$_3$ to the fact that more rigid Al$_2$O$_3$ particles can protrude from the softer copper matrix and then slide on the worn surfaces during rubbing, consequently increasing the COF of the composites [30].

5 Conclusion

1. The copper nanocomposites were successfully fabricated at 750 °C for 35 min by the hot pressing technique.
2. The Raman analysis shows that molybdenum disulfide did not transform into single layers because the proportion of molybdenum disulfide involved in the mixing process was high.
3. The density was decreased by adding both alumina and the mixture of alumina/MoS$_2$ for their low density and the formation of oxides on the grain boundaries.
4. Mixing alumina with copper for 15 h and cold-hot pressing led to a reduction in the size of the particles, as indicated by the microstructure.
5. The microstructure of the Cu/(Al$_2$O$_3$–MoS$_2$) sample shows that the MoS$_2$ was separated into flakes due to mixing it with copper for 15 h.
6. The hardness was improved by adding alumina and (Al$_2$O$_3$–MoS$_2$), and the last sample recorded 175.45 MPa with an improvement of 82.57% compared to the pure copper sample.
7. The mechanical wear rate was decreased, and the sample containing (Al$_2$O$_3$–MoS$_2$) recorded 2.6 mg compared to 22 mg for copper at 50 N load.
8. The coefficient of friction decreased by adding alumina and hybrid (Al$_2$O$_3$–MoS$_2$), and the last sample recorded 0.17 μm compared to 0.23 μm for pure copper at a load of 50 N.

Availability of data and material Not applicable.

Code availability Not applicable.

Declaration

Conflict of interest No conflict of interest related to this work.

References

1. Holmberg, K.; Andersson, P.; Erdemir, A. Global energy consumption due to friction in passenger cars. Tribol. Int., 47, 221–234, 2012.
2. K.H. Cho, U.S. Hong, K.S. Lee, H. Jang, Tribological properties and electrical signal transmission of copper–graphite composites, Tribology Letter, 27, 301–306, 2007.
3. X.C. Ma, et al., Sliding wear behavior of copper-graphite material for use in maglev transportation system, Wear, 265, 1087-1092, 2008
4. M. A. Elmaghraby, Hossam M. Yehia, Omayma A. Elkady, A. Abu-Oqail, Effect of Graphene Nano-Sheets Additions on the Microstructure and Wear Behavior of Copper Matrix Nano-Composite, Journal of Petroleum and Mining Engineering, Pp. 124-130, 2018.
5. S. Huang,Y. Feng, H. Liu, K. Ding, G. Qian, Electrical sliding friction and wear properties of Cu-MoS$_2$-graphite-WS$_2$ nanotubes composites in air and vacuum conditions, Materials Science & Engineering A 560, 685–692, 2013.
6. H. Cao, et al., Tribological behavior of Cu matrix composites containing graphite and tungsten disulfide, Tribology Transactions, 57: 1037-1043, 2014.
7. B. Radisavljevic, et al., Single-layer MoS$_2$ transistors. Nature Nanotechnology, **6**(3): p. 147-150, 2011.
8. T.W. Scharf, S.V. Prasad, Solid lubricants: a review, Journal of Materials Science 48, 511–531, 2013.
9. A.M. Kovalchenko, O.I. Fushchich, S. Danyluk, The tribological properties and mechanism of wear of Cu-based sintered powder materials containing molybdenum disulfide and molybdenum diselenite under unlubricated sliding against copper, Wear 290–291,106–123, 2012.
10. Hossam M Yehia, A Abu-Oqail, Maher A Elmaghraby, Omayma A Elkady, Microstructure, hardness, and tribology properties of the (Cu/MoS$_2$)/graphene nanocomposite via the electroless deposition and powder metallurgy technique Journal of Composite Materials, 54, Pp. 3435-3446, 2020.
11. Jin-Kun Xiao, Wei Zhang, Li-Ming Liu, Lei Zhang, Chao Zhang, Tribological behavior of copper-molybdenum disulfide composites, Wear, 384–385, 15, Pp. 61-71, 2017.
12. M. Nour-Eldin, O, A. Elkady, H. M. Yehia, H.M. Timeless Powder Hot Compaction of Nickel-Reinforced Al/(Al2O3-Graphene Nanosheet) Composite for Light Applications Using Hydrazine Reduction Method. J. of Materi Eng and Perform (2022).
13. H. M. Yehia, Microstructure, physical and mechanical properties of the Cu/ (WC-TiC-Co) nano-composites by the electro-less coating and powder metallurgy technique, Journal of Composite Materials, 53, pp. 1963-1971, 2019.
14. O. El-Kady., H. M. Yehia, Fathy. N. Preparation and characterization of Cu/ (WC-TiC-Co)/graphene nano-composites as a suitable

15. H.M. Yehia, et al., Microstructure, Hardness, Wear, and Magnetic Properties of (Tantalum, Niobium) Carbide-Nickel–Sintered Composites Fabricated from Blended and Coated Particles, Mater. Perform. Character. 4 (2020), 2379-1365.
16. H. M. Zidan, et al., Investigation of the Effectuation of Graphene Nanosheets (GNS) Addition on the Mechanical Properties and Microstructure of S390 HSS Using Powder Metallurgy Method, International Journal of Materials Technology and Innovation, 1, Pp. 52-57, 2021.
17. A. Omayma et al., Direct Observation of Induced Graphene and SiC Strengthening in Al-Ni alloy Via Hot pressing Technique, *Crystals*, *11*(9), 1142, 2021.
18. A. Tantawy, O. A. El Kady, H. M. Yehia, I. M. Ghayad, Effect of Nano ZrO$_2$ Additions on the Mechanical Properties of Ti-12Mo Composite by Powder Metallurgy Route. Key Engineering Materials, 835, 367–373, 2020.
19. K. Mehar, P. K. Mishra, S. K. Panda Numerical investigation of thermal frequency responses of graded hybrid smart nanocomposite (CNT-SMA-Epoxy) structure, Mechanics of Advanced Materials and Structures, 28:21, 2242-2254, 2021.
20. K. Mehar, S. K. Panda, N. Sharma, Numerical investigation and experimental verification of thermal frequency of carbon nanotube-reinforced sandwich structure, Engineering Structures 211, 110444, 2020.
21. Yehia HM, Nouh F, El-Kady OA, El-Bitar T Compos Mater,(in press).
22. P. Sahu, N. Sharma, H. Chand Dewangan, S. Kumar Panda, Thermo-Mechanical Transient Flexure of Glass-Carbon-Kevlar-Reinforced Hybrid Curved Composite Shell Panels: An Experimental Verification, International Journal of Applied Mechanics, 2150120, 2022.
23. Hong Li et al., From Bulk to Monolayer MoS$_2$: Evolution of Raman Scattering, Adv. Funct. Mater. 2012, 22, 1385–1390.7
24. B. C. Windom, W. G. Sawyer, D. W. Hahn, A Raman Spectroscopic Study of MoS$_2$ and MoO$_3$: Applications to Tribological Systems, Tribol Lett (2011) 42:301–310
25. R. Thiraviam, Development of copper: alumina Metal Matrix Composite by Powder Metallurgy method, Int. J. Materials and Product Technology, Vol. 31, Nos. 2/3/4, 2008.
26. S. Greco, K. Gutzeit, H. Hotz, et al. Selective laser melting (SLM) of AISI 316L—impact of laser power, layer thickness, and hatch spacing on roughness, density, and microhardness at constant input energy density. Int. J. Adv. Manuf. Technol. 108, 1551–1562 (2020).
27. Yu Pan et al., Tribological and mechanical properties of copper matrix composites reinforced with carbon nanotube and alumina nanoparticles, Mater. Res. Express 6 116524, 2019.
28. H. M. Yehia, P. Nyanor, W. M. Daoush, Characterization of Al-5Ni-0.5Mg/x (Al$_2$O$_3$-GNs) nanocomposites manufactured Via Hot Pressing Technique, materials characterization, 191, 112139, 2022.
29. Jin-Kun Xiao, Tribological behavior of copper-molybdenum disulfide composites, Wear, V. 384–385, (2017), 61-71.
30. CuiG J., BiQ L., Yang J., Liu W. M., Fabrication and study on tribological characteristics of bronze-alumina-silver composite under sea water condition Mater. Des. 46. (2013), 473–84

material for heat sink by powder metallurgy method, Refractory Metals & Hard Materials, 79, Pp. 108-114, 2019.